


A.A. FRESCHI<sup>1</sup>,  
P.V. DOS SANTOS<sup>2</sup>  
J. FREJLICH<sup>2</sup>

# Strong and fast phase modulation for quantitative analysis of photorefractive gratings

<sup>1</sup> Departamento de Física, IGCE, Universidade Estadual Paulista – UNESP, Caixa Postal 178, 13500-970, Rio Claro, SP, Brazil  
<sup>2</sup> Laboratório de Óptica, IFGW, Universidade Estadual de Campinas – UNICAMP, Caixa Postal 6165, 13083-970, Campinas, SP, Brazil

Received: 19 September 2005/  
Revised version: 12 January 2006  
Published online: 7 March 2006 • © Springer-Verlag 2006

**ABSTRACT** A new approach for studying photorefractive gratings in two-wave mixing experiments by a phase modulation technique is presented. The introduction of a large-amplitude, high-frequency sinusoidal phase modulation in one of the input beams blurs the interference pattern and provides powerful harmonic signals for accurate measurements of the grating diffraction efficiency  $\eta$  and the output phase shift  $\varphi$  between the transmitted and diffracted waves. The blurring of the light fringes can be used to suppress the higher spatial harmonics of the grating, allowing a space-charge field with sinusoidal profile to be recorded. Although the presence of such a strong phase modulation affects the beam coupling in a rather complicated way, it is shown that for the special case of equal intensity input beams, the effect of the phase modulation on  $\eta$  and  $\varphi$  is reduced to a weakening of the coupling strength. The potentialities of the technique are illustrated in a study of refractive-index waves excited by running interference patterns in a  $\text{Bi}_{12}\text{TiO}_{20}$  crystal. Expressions for the diffraction efficiency and the output phase shift are derived and used to match numerically calculated curves to the experimental data. The theoretical model is supported by the very good data fitting and allows the computation of important material parameters.

PACS 42.40.Ht; 42.40.Kw; 42.70.Nq

## 1 Introduction

Holograms are recorded in photorefractive crystals via photoexcitation of charge carriers (electrons and/or holes), which then form a volume space-charge electric field in the crystal [1, 2]. This field modulates the refractive index via the linear electrooptic (Pockels) effect. The refractive-index modulation is actually a phase volume hologram providing light diffraction. Relevant quantities like the diffraction efficiency  $\eta$  and the phase shift  $\varphi$  between transmitted and diffracted waves can be experimentally measured by using holographic techniques, which are very powerful tools for

materials' characterization [3, 4]. With the progress of the fields, a variety of holographic techniques were developed, improved, or adapted to solve specific problems concerning photorefractive materials.

There are several papers reporting the use of a high-frequency (fast) sinusoidal phase modulation in one of the recording beams for computing  $\eta$  or  $\varphi$  from the harmonic components that appear in the light output intensities [3–12]. Most published reports use a small-amplitude (weak) modulation in order not to disturb the holographic recording and to avoid the complications raised by the introduction of the phase modulation on the beam coupling. Weak modulations however may lead to poor signal-to-noise ratio of the harmonic terms that are detected. Throughout this paper the terms 'fast' or 'slow' refer to the inverse hologram response time and the terms 'weak' or 'strong' mean, respectively, that the effect of the phase modulation on the beam coupling properties can or cannot be neglected.

In a recent paper [12] Ringhofer et al. formulated the general theory for two-wave mixing in the presence of strong and fast phase modulation. They showed that the usual expression for  $\eta$  obtained by Kukhtarev et al. [13] is modified under the presence of strong periodic modulations. In the present paper we apply the developed theory to show that the output phase shift  $\varphi$  is modified, too. We also show that for the case of equal intensity input beams, the expressions for  $\eta$  and  $\varphi$  become very simple, with the strong phase modulation producing a weakening of the coupling constant. The use of a strong modulation greatly improves the detection sensitivity of the technique due to the powerful harmonic signals that are produced. At the same time, as the grating modulation is reduced, it provides a simple way to record photorefractive gratings in the linear writing regime (sinusoidal profile of the refractive-index modulation).

## 2 Diffraction efficiency and output phase shift

In the following we present the general steady-state solutions of the grating diffraction efficiency  $\eta$  and the output phase shift  $\varphi$  in the presence of a strong and fast phase modulation (Sect. 2.1), discuss the influence of the light absorption

✉ Fax: +55-19-3526-2238, E-mail: afreschi@rc.unesp.br

(Sect. 2.2), and treat the particular case of equal intensity input beams (Sect. 2.3).

### 2.1 Steady-state solutions

We carry out two-wave mixing experiments in the symmetric transmission geometry. Analogous to [9, 11, 12], we can express the complex amplitudes of the reference and signal beams in the form

$$\begin{aligned} R &= R_0 \mathcal{R}_r + S_0 \exp(i\psi \sin \omega t) \mathcal{R}_s, \\ S &= R_0 \mathcal{R}_r + S_0 \exp(i\psi \sin \omega t) \mathcal{R}_s. \end{aligned} \quad (1)$$

Here  $R_0$  and  $S_0 \exp(i\psi \sin \omega t)$  are the input amplitudes of the  $R$  and  $S$  beams, respectively, with  $i = \sqrt{-1}$ , and  $\mathcal{R}_r$ ,  $\mathcal{R}_s$ ,  $\mathcal{R}_s$ , and  $\mathcal{R}_r$  are dimensionless complex coefficients. The inputs  $R_0$  and  $S_0$  are generally slowly varying functions of time, and the term  $\psi \sin \omega t$  describes a sinusoidal phase modulation with angular frequency  $\omega$  much larger than the inverse of the grating response time ( $\omega \tau_{sc} \gg 1$ ). From the fundamental equations that describe the mutual Bragg diffraction of the  $R$  and  $S$  beams, one can easily show that  $\mathcal{R}_r = \mathcal{R}_s^*$  and  $\mathcal{R}_s = -\mathcal{R}_r^*$ , with the asterisk meaning the complex conjugate. The quantity  $\eta = |\mathcal{R}_s|^2 = |\mathcal{R}_r|^2 = 1 - |\mathcal{R}_r|^2 = 1 - |\mathcal{R}_s|^2$  is nothing else than the diffraction efficiency of the grating.

Apart from a constant conversion factor, the light intensities in the two output directions can be written as

$$\begin{aligned} I_R &= |R|^2 = I_R^0(1 - \eta) + I_S^0\eta + 2\Re \{ R_0^* \mathcal{R}_r^* S_0 \mathcal{R}_s e^{i\psi \sin \omega t} \}, \\ I_S &= |S|^2 = I_R^0\eta + I_S^0(1 - \eta) - 2\Re \{ R_0^* \mathcal{R}_r^* S_0 \mathcal{R}_s e^{i\psi \sin \omega t} \}, \end{aligned} \quad (2)$$

where  $\Re\{\}$  means the real part of the expression, and  $I_R^0 = |R_0|^2$  and  $I_S^0 = |S_0|^2$  are the input light intensities. The general formulation for the steady-state diffraction efficiency in the presence of fast phase modulation is calculated in [12] as

$$\eta = \frac{m_0^2 (1 - w_0^2)}{2g} \frac{\cosh(\gamma''d) - \cos(\gamma'd)}{g \cosh(\gamma''d) + w_0 \sinh(\gamma''d)}, \quad (3)$$

where  $m_0 = J_0(\psi)$  is the first-kind Bessel function of order zero with argument  $\psi$ , the term  $1 - w_0^2$  is the square of the input fringe contrast, with  $w_0 = (I_R^0 - I_S^0)/(I_R^0 + I_S^0)$  the normalized intensity difference of the input waves ( $-1 \leq w_0 \leq 1$ ),  $g = \sqrt{m_0^2 + w_0^2(1 - m_0^2)}$  is a positive factor ( $0 \leq g \leq 1$ ),  $d$  is the crystal thickness, and  $\gamma = \gamma' + i\gamma'' = |\gamma| \exp(i\phi)$  is a parameter (sometimes called the complex coupling coefficient) that characterizes the type and strength of the photorefractive response. The imaginary part  $\Im\{\gamma\} = \gamma''$  is responsible for the amplitude coupling (energy exchange) whereas the real part  $\Re\{\gamma\} = \gamma'$  is responsible for the phase coupling between the interfering beams. The amplitude of the coupling coefficient is proportional to the parameter  $g$  ( $|\gamma| \propto g$ ) [12], and the value  $\phi = \arg(\gamma)$  is the phase shift between the interference pattern and the grating;  $\phi$  is 0 or  $\pi$  in the case of local photorefractive response, and  $\phi = \pm\pi/2$  for nonlocal response.

Using the theory described in [12], and writing the transmitted and diffracted waves of the  $R$  beam in the form  $R_0 \mathcal{R}_r = \sqrt{I_R^0(1 - \eta)} \exp(i\varphi_R)$  and  $S_0 \mathcal{R}_s = \sqrt{I_S^0\eta} \exp(i\varphi_S)$ ,

the steady-state output phase difference  $\varphi = \varphi_R - \varphi_S = -\arg(R_0^* \mathcal{R}_r^* S_0 \mathcal{R}_s)$  can be written as

$$\begin{aligned} \tan \varphi &= - \frac{\sin(\gamma'd)}{\sinh(\gamma''d) + \frac{fI_R^0 - m_0^2 I_S^0}{g(I_R^0 + m_0^2 I_S^0)} [\cosh(\gamma''d) - \cos(\gamma'd)]}, \end{aligned} \quad (4)$$

with  $f = m_0^2 + w_0(1 - m_0^2)$  ranging from  $-1$  to  $1$ . The analysis of (3) and (4) shows that the influence of the fast phase modulation on the beam coupling properties depends on the value of the zero-order Bessel function  $m_0$ , which also appears in the parameters  $f$  and  $g$ . Note that in the absence of fast phase modulation ( $\psi = 0$ ),  $m_0 = f = g = 1$ , and the expressions for  $\eta$  (3) and  $\varphi$  (4) transform into the known results of [9].

The knowledge of the dependence of  $\gamma$  on the variable experimental conditions reveals information on the mechanisms of charge transfer and allows determining important material parameters. In the simple case of one photoactive center, one charge carrier, no photovoltaic effect, and taking the first spatial-harmonic approximation, the steady-state value of the coupling coefficient is given by [11, 12]

$$\gamma = g \frac{\pi n^3 r_{\text{eff}} (E_0 + iE_D)}{\lambda \left[ 1 - i \frac{\varepsilon \varepsilon_0}{e N_{\text{eff}}} K(E_0 + iE_D) \right] - i\Omega \frac{\varepsilon \varepsilon_0 h\nu}{e \alpha I \Phi} \left[ \frac{1}{\mu\tau} - iK(E_0 + iE_D) \right]}, \quad (5)$$

where  $n$  is the average index of refraction,  $r_{\text{eff}}$  is the effective electrooptic coefficient,  $\lambda$  is the light wavelength,  $E_0$  is an externally applied electric field,  $E_D = Kk_B T/e$  is the diffusion field,  $k_B$  is the Boltzmann constant,  $T$  is the absolute temperature,  $e$  is the elementary charge,  $\varepsilon$  is the static relative permittivity,  $\varepsilon_0$  is the electric permittivity of vacuum,  $\Omega = Ku$  ( $K$  the grating wave number and  $u$  the grating speed),  $h\nu$  is the photon energy,  $\alpha$  is the bulk absorption, and  $I = (I_R^0 + I_S^0)(1 - R) \cos(\theta) \exp(-\alpha z)$  is the average overall irradiance inside the sample, with  $1 - R$  the front surface transmittance,  $\theta$  the angle of incidence of the beams, and  $z$  the spatial coordinate along the crystal thickness. Other parameters are the effective trap concentration  $N_{\text{eff}}$ , the quantum efficiency  $\Phi$  for photoexcitation, and the mobility–lifetime product  $\mu\tau$  for the photoexcited charge carriers.

### 2.2 Including light absorption

In low-absorbing materials the average light intensity  $I$  in (5) is nearly constant through the crystal thickness. However, when light absorption becomes appreciable, it is required to take into account the exponential decay of  $I$ , which causes the dielectric relaxation time to vary along the crystal. Consequently, the theory developed for an absorptionless crystal can only be applied for very thin crystal slabs (along the direction of the light propagation), so as to consider the light intensity constant within the slab. For thick crystals, the correct result is obtained by numerically integrating the analytical solution for a thin slab over the entire crystal thickness  $d$ . This is accomplished by substituting  $\gamma'$  and  $\gamma''$  by their

averages [11, 14],

$$\bar{\gamma}' = (1/d) \int_0^d \gamma' dz \text{ and } \bar{\gamma}'' = (1/d) \int_0^d \gamma'' dz.$$

### 2.3 Input beams with equal intensities

The general relations obtained so far are valid for any input fringe contrast  $(1 - w_0^2)^{1/2}$ . There is however a very favorable situation for instrumental applications of the fast phase modulation technique, namely the condition of equal input intensities ( $w_0 = 0$ ). This condition leads to especially simple expressions for  $\eta$  and  $\varphi$  and allows controlling the ‘effective contrast’ of the light fringes (as ‘seen’ by the material) through the modulation amplitude  $\psi$ . In particular, the linear writing regime (sinusoidal shape for the spatial modulation of the refractive index) can be achieved by using a strong modulation so as to ensure that  $|m_0| \ll 1$ . The condition  $I_R^0 = I_S^0$  implies that  $w_0 = 0$ ,  $g = m_0$ , and  $f = m_0^2$ , which substituted into (3) and (4) result in

$$\eta = \frac{1}{2} \left[ 1 - \frac{\cos(\gamma'd)}{\cosh(\gamma''d)} \right] \approx (1/4) |\gamma d|^2, \quad (6)$$

$$\tan \varphi = -\frac{\sin(\gamma'd)}{\sinh(\gamma''d)} \approx -\frac{\gamma'}{\gamma''}. \quad (7)$$

Here, the first solutions are the exact ones, whereas the approximations are valid for small grating modulations and/or sufficiently thin crystals ( $|\gamma d| \ll 1$ ). One sees that within the validity of the approximate solutions, the effect of the fast phase modulation is reduced to a weakening of the diffraction efficiency proportional to  $m_0^2$  ( $|\gamma| \propto g$ ), whereas it has no effect on the output phase shift  $\varphi$ .

In the absence of fast phase modulation, the solutions for  $\eta$  and  $\varphi$  can be found using the well-known theory developed by Kukhtarev et al. [13]: the formation of the space-charge field is modeled based on the material parameters, and  $\eta$  and  $\varphi$  are calculated using a proper formulation for the electrooptic effect and the coupled wave theory. Under the condition  $w_0 = 0$  and neglecting the photovoltaic effect, the obtained solutions have identical structures to those in (6) and (7). The remarkable difference is the appearance of the term  $g$  ( $= m_0$ ) in the coupling coefficient  $\gamma$ .

## 3 Experiment

Due to the dynamic nature of the recording process in photorefractive materials, hologram writing can take place both in the stationary regime (stationary light pattern) or under nonstationary conditions (moving light pattern). The interest in studying moving gratings relies, among other reasons, on the resonant nature of grating strength [15, 16]. In order to illustrate the potentialities of the technique, an experiment aiming to characterize some important photorefractive parameters in a nominally undoped  $\text{Bi}_{12}\text{TiO}_{20}$  (BTO) crystal is reported below.

### 3.1 Experimental method

The general scheme of the holographic setup is illustrated in Fig. 1. Experiments are carried out at the room temperature  $T = 296$  K. The light source is an argon-ion laser operated at the wavelength  $\lambda = 514.5$  nm. The coherent and collimated  $R$  and  $S$  waves have equal intensities  $I_R^0 = I_S^0 = I_0 = 13$  mW/cm<sup>2</sup> and intersect symmetrically in the BTO crystal with an incident angle  $\theta$  to record a grating with wave number  $K = (4\pi/\lambda) \sin \theta$ . The grating vector  $\mathbf{K} = K\hat{x}$  lies in the  $x$ -direction, perpendicular to the crystallographic (001)-axis (parallel to the  $y$ -direction), and the  $xy$  plane corresponds to the (110) crystal face. The BTO sample (BTO-8) is  $d = 0.95$ -mm thick (along the  $z$ -coordinate), the bulk refractive index is  $n = 2.6$ , the optical activity is  $\varrho = 10.8^\circ/\text{mm}$ , the static relative permittivity is  $\varepsilon = 47$ , the effective electrooptic coefficient is  $r_{\text{eff}} = 5.6$  pm/V, and the total (bulk + light-induced) intensity absorption coefficient is  $\alpha = 1.7$  mm<sup>-1</sup>. An external dc voltage  $V_0 = 4.55$  kV is applied through silver paint electrodes, resulting in an electric field  $E_0$  parallel to the grating vector. The value of this field in the region of measurement can be written as  $E_0 = \xi V_0/l = \xi \times 9.58$  kV/cm, with  $l = 4.75$  mm the distance between the electrodes and  $\xi$  a dimensionless parameter that must be determined empirically. The orientation of the linear light input polarization is chosen so as to be at  $45^\circ$  to the (001)-axis in the middle slice of the sample. This orientation prevents practically any change in the linear state of polarization due to the induced birefringence and results in parallel polarized trans-

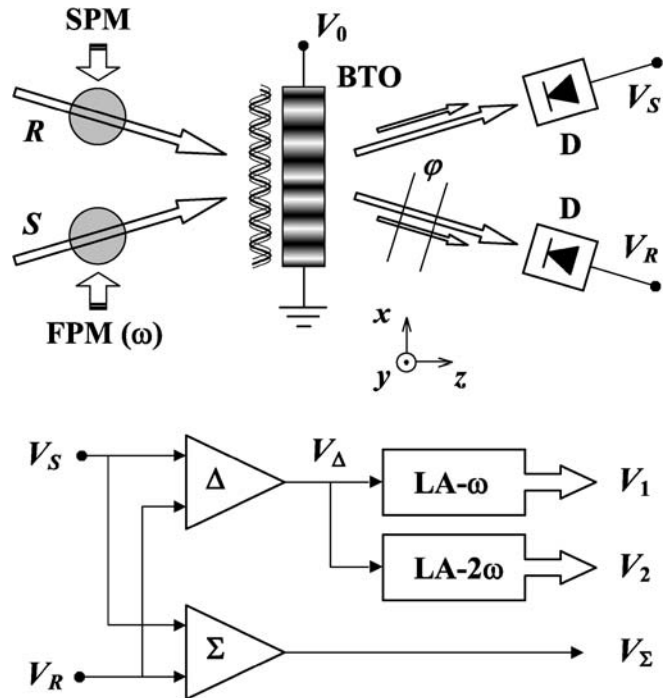


**FIGURE 1** Experimental setup.  $R$  and  $S$ : collimated light beams; FPM: strong and fast sinusoidal phase modulation at  $\omega$ ; SPM: slow phase modulation used to move the interference pattern at constant speed;  $V_0$ : applied dc voltage; BTO: photorefractive crystal;  $\varphi$ : phase shift between the transmitted and diffracted waves; D: identical photodetectors;  $V_\Delta = V_R - V_S$  and  $V_\Sigma = V_R + V_S$ ; LA- $\omega$  and LA- $2\omega$ : lock-in amplifiers tuned to  $\omega$  and  $2\omega$ ;  $V_1$ ,  $V_2$ , and  $V_\Sigma$ : output signals used for signal processing

mitted and diffracted beams in the two output directions [17]. Also, the results predicted by the scalar theory of diffraction can be applied in the present case because optical activity can be neglected ( $\rho d \ll |\gamma d|$ ) [18].

Two identical photodetectors with bandwidth  $BW \gg \omega$  are used to transform the output intensities of the  $R$  and  $S$  waves (2) into the voltages  $V_R = \kappa I_R$  and  $V_S = \kappa I_S$ , with  $\kappa$  an intensity-to-voltage conversion factor. The collected light waves come from the central region of the crystal and the voltages  $V_\Delta = V_R - V_S$  and  $V_\Sigma = V_R + V_S$  are generated. Two phase modulators are employed in our setup (see Fig. 1). The  $S$  beam is phase modulated with a strong ( $\psi = 1.80$  radians) and fast ( $\omega = 2\pi \times 1600$  radians/s) sinusoidal signal, whereas a slow linear phase scanning is introduced in the  $R$  beam. The aim of the slow phase scanning is to control the velocity  $\mathbf{u} = u\hat{x}$  of the running grating. This is equivalent to producing a constant frequency detuning  $\Omega = Ku$  in the  $R$  beam. Due to the fast phase modulation, the Fourier spectrum of the voltage  $V_\Delta$  presents several harmonic terms of the fundamental frequency  $\omega$ . The  $\omega$ -tuned lock-in amplifiers measure respectively the first- and second-harmonic terms,  $V_\Delta^\omega \sin \omega t$  and  $V_\Delta^{2\omega} \cos 2\omega t$ , and give outputs in the form of dc (or slowly varying) voltages proportional to the value of the ac signal being measured. Most lock-in amplifiers apply a proportionality factor to give the root-mean-square amplitude of the ac signal, so that we can write  $V_1 = V_\Delta^\omega / \sqrt{2} = -4\sqrt{2}\kappa m_1 \sqrt{I_R^0 I_S^0} \sqrt{\eta(1-\eta)} \sin \varphi$  and  $V_2 = V_\Delta^{2\omega} / \sqrt{2} = 4\sqrt{2}\kappa m_2 \sqrt{I_R^0 I_S^0} \sqrt{\eta(1-\eta)} \cos \varphi$ , with  $m_q = J_q(\psi)$  the first-kind Bessel function of order  $q$  with argument  $\psi$ . It follows that the diffraction efficiency and output phase shift can be determined from the voltages  $V_1$ ,  $V_2$ , and  $V_\Sigma$  using the relations

$$\sqrt{\eta(1-\eta)} = \frac{\sqrt{(V_1/m_1)^2 + (V_2/m_2)^2}}{2\sqrt{2}V_\Sigma} \quad \text{and} \quad (8)$$

$$\tan \varphi = -\frac{m_2 V_1}{m_1 V_2}.$$

The diffraction efficiency computed from (8) is equivalent to the ratio between the diffracted and the sum of the diffracted and transmitted light intensities generated by a single beam entering the crystal under the Bragg angle. In fact, homogeneous light losses due to absorption, scattering, and surface reflections are not considered in our definition of  $\eta$ ; all these losses (as well as the conversion factor  $\kappa$ ) affect proportionally the voltages  $V_1$ ,  $V_2$ , and  $V_\Sigma$ , and therefore cancel out when computing  $\eta$  and  $\varphi$ . Note that if the setup is desired to operate around  $m_1 \approx 0$  (or  $m_2 \approx 0$ ), the lock-in amplifier LA- $\omega$  (or LA- $2\omega$ ) can be tuned to another odd (or even) harmonic component of the fundamental frequency  $\omega$ , such as the third (or fourth) one. Equations (8) remain valid as long as the corresponding subscripts are changed. It is also worth mentioning that local photochromic gratings (which may become significant at small spatial frequencies [19]) are suppressed from the measurements when the signals from the two photodetectors are subtracted [5, 20]. Conversely, the photorefractive grating is suppressed when the signals are added.

In our setup, a voltage signal drives a piezoelectrically supported mirror to produce the phase modulation  $\psi \sin \omega t$ .

We call  $V_M$  the amplitude of the applied  $\omega$ -signal and define  $V_\pi$  as the half-wave voltage of the phase modulator at  $\omega$ . Assuming that the modulator is operating in the linear regime we can write  $\psi = \pi(V_M/V_\pi)$ ; if  $V_\pi$  is known the amplitude  $\psi$  can be controlled through  $V_M$ . Experimentally,  $V_\pi$  can be measured by increasing  $V_M$  until the first root of the Bessel function  $m_1$  is found, when  $\psi \approx 3.83$  radians and  $V_1 = 0$  independently of the phase  $\varphi$  between the transmitted and diffracted waves. Unless otherwise noted, we use in this work a modulation amplitude  $\psi = (1.80 \pm 0.05)$  radians, so that  $m_0 = (0.34 \pm 0.03)$ ,  $m_1 = (0.582 \pm 0.002)$ , and  $m_2 = (0.306 \pm 0.012)$ . Assuming that the interfering beams are completely coherent and parallel-polarized, and that  $V_1$ ,  $V_2$ , and  $V_\Sigma$  are properly measured, the accuracy of the results depends on the uncertainties in the values of  $m_1$  and  $m_2$ , which are used to compute  $\eta$  and  $\varphi$  through (8). At  $\psi = 1.80$  radians the derivative  $dm_2/d\psi \gg dm_1/d\psi$  and maximum errors occur

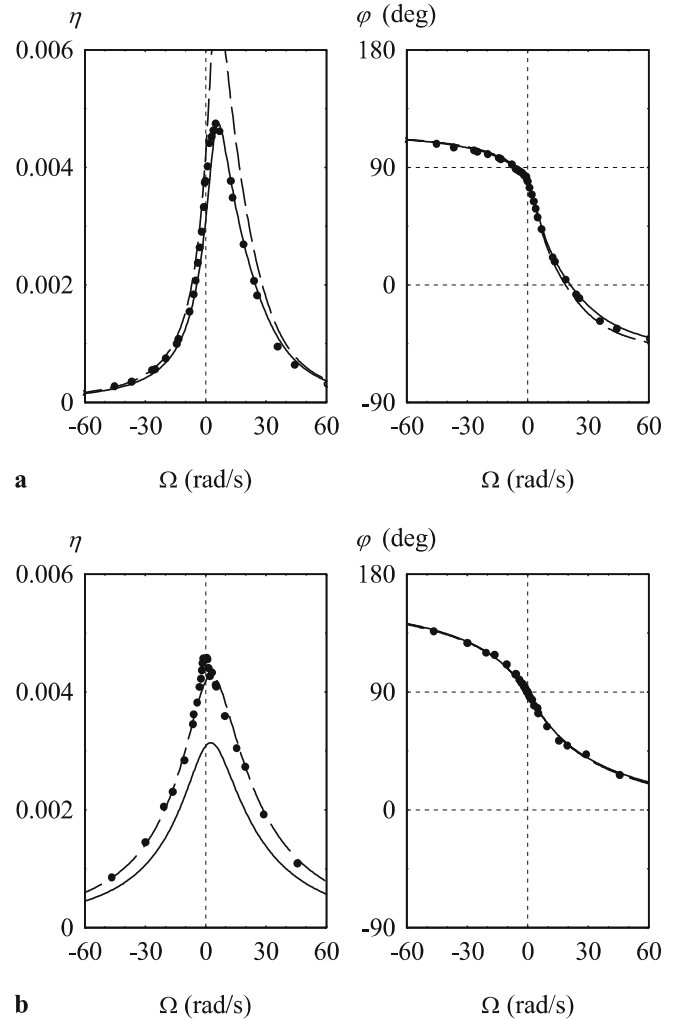


**FIGURE 2** Dependence of the diffraction efficiency  $\eta$  and the output phase shift  $\varphi$  on the frequency detuning  $\Omega = Ku$  for the spatial frequencies (a)  $K/2\pi = 640 \text{ mm}^{-1}$  and (b)  $K/2\pi = 76 \text{ mm}^{-1}$ . Experimental conditions: BTO-8 crystal; equal input intensities  $I_R^0 = I_S^0 = 13 \text{ mW/cm}^2$  ( $\lambda = 514.5 \text{ nm}$ ); fast phase modulation amplitude  $\psi = 1.80$  radians ( $m_0 = 0.34$ ); electric field  $E_0 = \xi \times 9.58 \text{ kV/cm}$ . The dots represent the experimental data, whereas the solid ( $\xi = 0.6$ ) and dashed ( $\xi = 0.7$ ) lines correspond to numerical calculations (see text)

around  $\varphi \approx 0$  or  $\pi$  ( $|V_2| \gg |V_1|$ ). In this condition, an error of  $\delta\psi = \pm 0.05$  radians leads to  $\delta\eta/\eta \approx \pm 8\%$  and  $\delta\varphi/\varphi \approx \pm 4\%$ . In practice, small electronic offsets may also need to be taken into account when measuring very weak signals, causing phase offset errors that are typically smaller than  $\pm 2^\circ$ .

### 3.2 Results

Figure 2 shows examples of the frequency detuning dependences of  $\eta$  and  $\varphi$  for two different grating wave numbers: (a)  $K = 4.02 \mu\text{m}^{-1}$  and (b)  $K = 0.48 \mu\text{m}^{-1}$ . The usual resonant behavior of the diffraction efficiency  $\eta$  on the frequency detuning  $\Omega$  is evident from the experimental data (dots). The small values observed for  $\eta$  allowed us to use the approximate solutions of (6) and (7) to perform the numerical calculations. Besides some fundamental constants, there are as many as 17 inputs, namely  $\lambda$ ,  $I_0$ ,  $\psi$ ,  $K$ ,  $u$ ,  $T$ ,  $V_0$ ,  $l$ ,  $d$ ,  $\alpha$ ,  $\varepsilon$ ,  $n$ ,  $r_{\text{eff}}$ ,  $\xi$ ,  $\mu\tau$ ,  $\Phi$ , and  $N_{\text{eff}}$ . Except for the material parameters  $\mu\tau$ ,  $\Phi$ , and  $N_{\text{eff}}$ , and the dimensionless field factor  $\xi$ , all other quantities are known with good accuracy. These four unknowns were determined by matching the theoretical curves to the data of  $\eta$  and  $\varphi$ . Because of the relatively large number (four) of fit parameters, it is helpful to choose a realistic set of initial guesses to perform the curve fit. A  $\xi$ -value in the range  $0.5 < \xi < 1$  is quite reasonable [21] considering that electrical charges associated with the photorefractive centers may accumulate near the electrodes and thereby act to screen the applied field. We also know that the relation  $0 \leq \Phi \leq 1$  must be fulfilled, and that the expected values for  $N_{\text{eff}}$  and  $\mu\tau$  in BTO crystals should be somewhere around  $N_{\text{eff}} \approx 10^{23} \text{m}^{-3}$  [11] and  $\mu\tau \approx 10^{-11} \text{m}^2/\text{V}$  [22]. The best-fit material parameters are then found to be  $\mu\tau = 0.6 \times 10^{-12} \text{m}^2/\text{V}$ ,  $\Phi = 0.29$ , and  $N_{\text{eff}} = 1 \times 10^{23} \text{m}^{-3}$ . These values were used to plot the solid and dashed lines in Fig. 2. The solid lines (best fit for Fig. 2a) use a factor  $\xi = 0.60$ , whereas the dashed ones (best fit for Fig. 2b) use a factor  $\xi = 0.70$ . Note that the two-wave mixing geometry usually causes the appearance of shadowed regions in the vicinity of the opaque electrodes of the crystal. These regions have higher resistivities than in the central area of the sample, where the measurement is taken. When the angle of incidence  $\theta$  is reduced, the volume of the shadowed regions decreases and the factor  $\xi$  is expected to increase, in accordance with the results.

Although a rigorous analysis of the uncertainties of the measured parameters is beyond the scope of this paper, the accuracy of the results was estimated by investigating the influence of the fit parameters on the theoretical curves. For a crude estimate, we might simply compare theoretical curves having different values for a specific fit parameter. As an example, the comparison between the solid and dashed lines in Fig. 2 illustrates the effect of a 0.1 variation in the field factor  $\xi$ . Using a similar procedure, we estimate an accuracy of about  $\pm 10\%$  for  $\mu\tau$  and  $\Phi$ , which are more related to characteristics of the resonance peak such as the frequency and quality factor (see Fig. 3). We also estimate  $N_{\text{eff}} \gtrsim 1 \times 10^{23} \text{m}^{-3}$ ;  $N_{\text{eff}}$  exerts a weak influence on the computed curves probably because we are working far from photoactive center saturation, which is mathematically translated into the conditions  $K^2 l_s^2 \ll 1$  and  $K l_E \ll 1$ , with  $l_s = \sqrt{\varepsilon \varepsilon_0 k_B T / e^2 N_{\text{eff}}} \lesssim 0.025 \mu\text{m}$  the Debye screening length

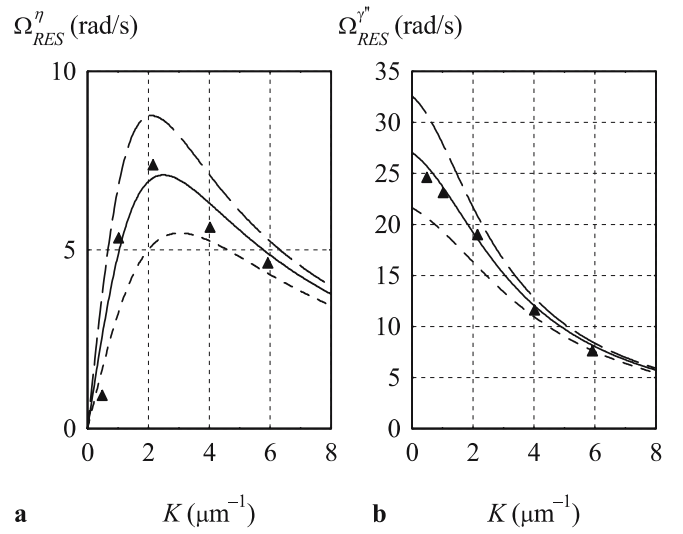


**FIGURE 3** Angular resonant frequencies  $\Omega_{\text{RES}} = K u_{\text{RES}}$  for (a)  $\eta$  and (b)  $\overline{\gamma}'$ , in dependence on the grating wave number  $K$  for the BTO sample. The *dots* are the experimentally measured values and the *solid curves* (best fits) are calculations using the theoretical formulas for these dependences, with the field factor  $\xi = 0.6$  and the material parameters determined from Fig. 2. The *dashed curves* are plotted to illustrate the influence of the mobility–lifetime product on the results ( $\mu\tau + 10\%$ : long dash and  $\mu\tau - 10\%$ : short dash)

and  $l_E = \varepsilon \varepsilon_0 E_0 / e N_{\text{eff}} \lesssim 0.015 \mu\text{m}$  the length of electron tightening by an electric field  $E_0 = 0.6 \times 9.58 \text{ kV/cm}$ . At this field the drift length  $L_E = \mu\tau E_0 \approx 0.35 \mu\text{m}$  and the diffusion length  $L_D = \sqrt{\mu\tau k_B T / e} \approx 0.12 \mu\text{m}$ .

Figure 3 presents the detuning frequencies that ensure the maximum diffraction efficiency ( $\Omega_{\text{RES}}^\eta$ ) and energy transfer ( $\Omega_{\text{RES}}^{\overline{\gamma}'}$ ) as functions of the grating wave number  $K$ . The dots depict the experimentally measured values at five different  $K$ 's normalized to a factor  $\xi = 0.60$  ( $\xi$  ranged from 0.60 to 0.70 in the investigated  $K$  range), where it is assumed for normalization that the frequency of resonance depends inversely on the electric field [22]. The solid lines are theoretical curves calculated with the material parameters reported above and  $\xi = 0.60$ . The agreement between theory and experiment may again be regarded as good. The long-dashed lines and the short-dashed lines correspond to the theoretical curves calculated for  $\mu\tau = 0.66 \times 10^{-12} \text{m}^2/\text{V}$  and  $\mu\tau = 0.54 \times 10^{-12} \text{m}^2/\text{V}$ , respectively ( $\pm 10\%$  variations). It is worth mentioning that  $\Omega_{\text{RES}}^\eta$  does not follow the  $1/K$  dispersion law obtained by other researchers using a BTO sample with a  $\mu\tau$  product roughly one order of magnitude larger [22]. The quite different values of the resonant frequencies  $\Omega_{\text{RES}}^\eta$  and  $\Omega_{\text{RES}}^{\overline{\gamma}'}$  can also be attributed to the relatively small  $\mu\tau$  of our BTO sample (short drift length condition) [23].

So far, we have only considered the experimental arrangement operating with  $\psi = 1.8$  radians ( $m_0 = 0.34$ ,  $m_1 = 0.58$ , and  $m_2 = 0.31$ ). In Fig. 4 we compare the behavior of  $\eta$  and  $\varphi$  at  $K = 4.02 \mu\text{m}^{-1}$  for two different effective contrasts  $m_0$ . To find a reference point, the dots ( $\bullet$ ) and the solid lines are the same as those plotted in Fig. 2a, while the + symbols are the data for a modulation amplitude  $\psi = 0.40$  radians ( $m_0 = 0.96$ ,  $m_1 = 0.20$ , and  $m_2 = 0.020$ ). An additional  $\eta$ -axis (one order of magnitude larger) was added to depict this new data set.

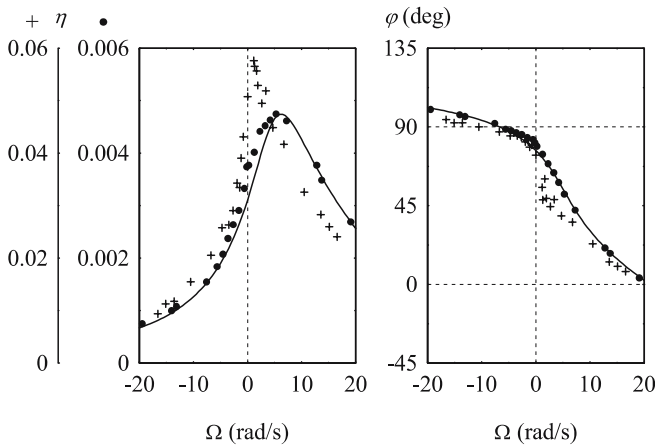


**FIGURE 4** Influence of higher spatial harmonics of the space-charge field on  $\eta$  and  $\varphi$ . The dots ( $\bullet$ ) and the solid lines are the same as those plotted in Fig. 2a, with  $\psi = 1.80$  radians ( $m_0 = 0.34$ ), whereas the + symbols are the experimental data for  $\psi = 0.40$  radians ( $m_0 = 0.96$ )

Note that  $\eta$  is described by a more asymmetric curve at larger contrasts because the higher spatial harmonics of the space-charge field  $E_{sc}$  become important [14, 24]. Also, the frequency of resonance  $\Omega_{RES}^\eta$  decreases from  $\approx 6$  radians/s at  $m_0 = 0.34$  to  $\approx 1$  radian/s at  $m_0 = 0.96$ . The  $\varphi$ -graph in Fig. 4 shows that the phase changes significantly with  $m_0$  in the region of resonance. Far from resonance, the higher spatial harmonics are unimportant and the fundamental component of  $E_{sc}$  suffices to describe the beam coupling correctly. It is worth mentioning that in both investigated cases  $m_2 < m_1$ , so that the detection sensitivity is limited by  $V_2 \propto m_2 \eta^{1/2}$ . Thus, assuming that the noise level remains unchanged when  $\psi$  is raised from 0.4 radians to 1.8 radians and that  $m_2$  increases  $\approx 15$  times, the minimum detectable  $\eta$  is decreased by a factor of  $\approx 200$ .

#### 4 Conclusions

Phase modulation techniques are useful tools for the determination of photorefractive parameters. The use of a strong sinusoidal phase modulation greatly improves the detection sensitivity of the technique when compared to experiments where weak modulations are employed. At the same time it provides a simple way to reduce the effective contrast of the light fringes, allowing index gratings with a sinusoidal profile to be recorded. The general expressions describing the beam coupling and the experimental procedure for measuring the grating diffraction efficiency and the

output phase shift are presented. These expressions are considerably simplified when equal intensity recording beams are used. The technique was applied to the study of running holograms in  $\text{Bi}_{12}\text{TiO}_{20}$  crystals and important crystal parameters were determined. The presented method is by no means restricted to the study of the classic photorefractive grating (build up of a space-charge field plus electrooptic effect). It can also be applied to measure the effects of additional gratings, such as thermal gratings and photochromic ones.

**ACKNOWLEDGEMENTS** The authors acknowledge the financial support from the Conselho Nacional de Desenvolvimento Científico e Tecnológico (CNPq; 540294/01-2), Brazil, and from the Fundação de Amparo à Pesquisa do Estado de São Paulo (FAPESP; 03/09915-0), Brazil.

#### REFERENCES

- 1 J. Feinberg, Phys. Today, October, 46 (1988)
- 2 L. Solymar, D.J. Webb, A. Grunnet-Jepsen, *The Physics and Applications of Photorefractive Materials* (Clarendon, Oxford, 1996)
- 3 K. Buse, Appl. Phys. B **64**, 273 (1997)
- 4 R.A. Rupp, Appl. Phys. A **55**, 2 (1992)
- 5 M. Gehrtz, J. Pinsi, C. Bräuchle, Appl. Phys. B **43**, 61 (1987)
- 6 P.M. Garcia, L. Cescato, J. Frejlich, J. Appl. Phys. **66**, 47 (1989)
- 7 R.S. Cudney, G.D. Bacher, R.M. Pierce, J. Feinberg, Opt. Lett. **17**, 67 (1992)
- 8 R. Hofmeister, A. Yariv, A. Kewitsch, S. Yagi, Opt. Lett. **18**, 488 (1993)
- 9 J. Frejlich, P.M. Garcia, K.H. Ringhofer, E. Shamonina, J. Opt. Soc. Am. B **14**, 1741 (1997)
- 10 A.A. Freschi, J. Frejlich, Opt. Lett. **20**, 635 (1995)
- 11 I. de Oliveira, J. Frejlich, J. Opt. Soc. Am. B **18**, 291 (2001)
- 12 K.H. Ringhofer, V.P. Kamenov, B.I. Sturman, A. Chernykh, Phys. Rev. E **61**, 2029 (2000)
- 13 N.V. Kukhtarev, V.B. Markov, S.G. Odulov, Ferroelectrics **22**, 949 (1979)
- 14 E. Shamonina, K.H. Ringhofer, P.M. Garcia, A.A. Freschi, J. Frejlich, Opt. Commun. **141**, 132 (1997)
- 15 P. Refregier, L. Solymar, H. Rajbenbach, J.P. Huignard, J. Appl. Phys. **58**, 45 (1985)
- 16 V.V. Bryksin, M.P. Petrov, Phys. Solid State **40**, 1317 (1998)
- 17 A. Marrakchi, R.V. Johnson, A.R. Tanguay, Jr., J. Opt. Soc. Am. B **3**, 321 (1986)
- 18 B.I. Sturman, D.J. Webb, R. Kowarschik, E. Shamonina, K.H. Ringhofer, J. Opt. Soc. Am. B **11**, 1813 (1994)
- 19 R.S. Cudney, R.M. Pierce, G.D. Bacher, J. Feinberg, J. Opt. Soc. Am. B **8**, 1326 (1991)
- 20 C.H. Kwak, S.J. Lee, Opt. Commun. **183**, 547 (2000)
- 21 A. Grunnet-Jepsen, I. Aubrecht, L. Solymar, J. Opt. Soc. Am. B **12**, 921 (1995)
- 22 M.P. Petrov, V.V. Bryksin, V.M. Petrov, S. Wevering, E. Kratzig, Phys. Rev. A **60**, 2413 (1999)
- 23 S.L. Sochava, E.V. Mokrushina, V.V. Prokofiev, S.I. Stepanov, J. Opt. Soc. Am. B **10**, 1600 (1993)
- 24 G. Brost, K.M. Magde, J.J. Larkin, M.T. Harris, J. Opt. Soc. Am. B **11**, 1764 (1994)